

PREDICTIVE MAPPING OF MINERAL PROSPECTIVITY IN AREAS WITHOUT KNOWN MINERAL DEPOSITS

Emmanuel John M. Carranza

International Institute for Geo-Information Science and Earth Observation (ITC)

Hengelosestraat 99, P.O. Box 6, 7500 AA Enschede, The Netherlands

(Email: carranza@itc.nl; Phone: +31.53.4874444; Fax: +31.53.4874336)

Introduction

In areas where a number of mineral deposits of the type sought have already been discovered, predictive mapping of other prospective zones involves scoring and integration of geological, geochemical, or geophysical evidences. The evidential scores represent strengths of spatial associations of individual evidences with discovered mineral deposits of the type sought. The higher the number of discovered deposits, the more robust are the evidential scores and the predictive map. Obviously, estimation of evidential scores for predictive mapping of mineral prospectivity in poorly explored geologically-permissive areas is difficult, especially if there are no or few discovered mineral deposits of the type sought. Geologically-permissive areas are those where the ensemble of geological features (lithologies, structures, etc.) represents inter-play of processes that plausibly favored mineral deposit formation. It has been demonstrated that data-driven predictive mapping of mineral prospectivity is viable in areas with few discovered mineral deposits of the type sought (Carranza, 2004). This paper presents an adaptation of the “wildcat” method proposed by Carranza and Hale (2002c) for predictive mapping of mineral prospectivity in areas with no discovered mineral deposits of the type sought.

Test area

The test area, of about 920 km², is in the province of Abra in northwestern Philippines. In this area, Bureau of Mines (1976) identified 12 porphyry-Cu prospects, while JICA (1980) mapped several mineralized zones with porphyry-Cu deposits and indications (Fig. 1). Descriptions of the geology and porphyry-Cu mineralization in the test area can be found in Carranza (2004). The known porphyry-Cu prospects and mineralized zones are not used to create a predictive map of porphyry-Cu prospectivity but only to validate the proposed methodology.

The following geological features used by Carranza (2004) as spatial

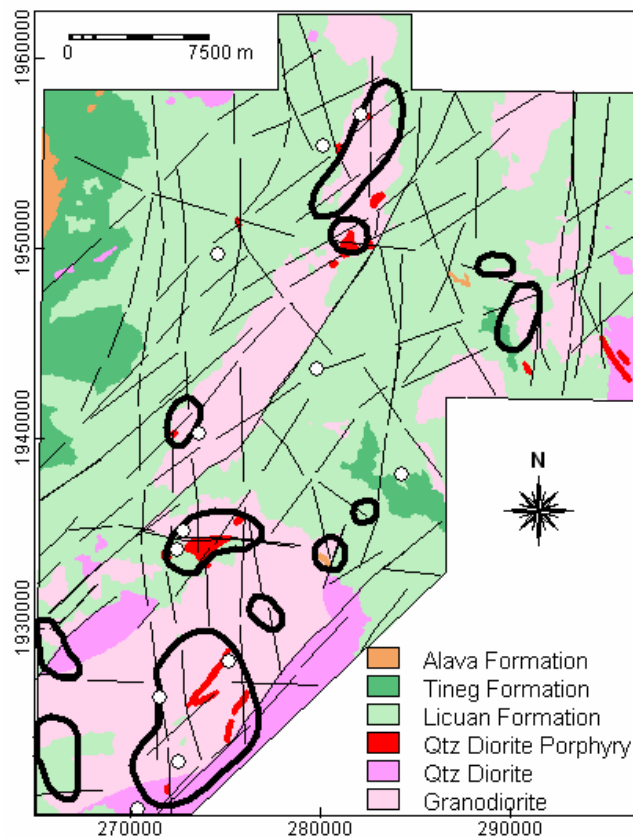


Fig. 1. Simplified geological map of test area (adapted from JICA, 1980). Black lines are faults. Circles are porphyry-Cu prospects (Bureau of Mines, 1976). Polygons in thick black lines are mineralized zones (JICA, 1980). Map coordinates are in meters (UTM projection, zone 51).

evidences of porphyry-Cu prospectivity were also used in this study: (a) granodiorite batholith margins, (b) quartz diorite batholith margins, (c) quartz diorite porphyry stock centroids, (d) NW-trending faults, (e) NE-trending faults, (f) N-trending faults, and (g) intersections of N- and NE-trending faults. In addition, drainage sample catchment basins with Cu anomalies (Carranza, 2004) were used as evidence.

Modified wildcat technique

Geological features or geochemical anomalies associated genetically with certain mineral deposits can be expected to exhibit spatial association with such mineral deposits (Carranza and Hale, 2002a). Accordingly, predictive mapping of mineral prospectivity in poorly-explored areas can exploit evidential maps based on proximity to map features considered as controls or manifestations of mineral deposits of interest (Carranza and Hale, 2002c). Thus, maps of distance to a set of geological features are created first. These continuous data maps are then discretized into proximity classes using equal-percentile distance intervals, because percentile classification is robust for continuous data of any statistical distribution. In a proximity class map p ($=1,2,\dots,n$), an evidential class score Sc is calculated for every proximity class c ($=1,2,\dots,m$), viz.:

$$Sc = \frac{1}{\tilde{d}_c} h \quad (\text{Eq. 1})$$

where \tilde{d}_c is class median distance and h is pixel hypotenuse. For example, using a pixel size of 100 m, a proximity class with median distance of 250 m will have an evidential score of 0.564 (i.e., $1 \div 250 \times 141$). The class median distance is used instead of the class mean distance, because median is a more robust estimation of central data tendency especially if statistical structure of data and its statistical association with target variable (i.e., mineral deposits) are unknown. This scheme of evidential scoring (Carranza, 2004) results in evidential scores that decrease exponentially with decreasing proximity to geological features, suggesting that mineral deposits preferentially occur only in zones highly proximal to geological features. This is not generally realistic, because in many examples of data-driven predictive mapping of mineral prospectivity evidential weights tend to decrease parabolically rather than exponentially with decreasing proximity to geological features (Fig. 2). Thus, it is proposed to apply the logistic fuzzy membership function used by Porwal *et al.* (2003), viz.:

$$fSc = \frac{1}{1 + e^{-m(Sc - \tilde{S}_p)}} \quad (\text{Eq. 2})$$

where fSc is fuzzified evidential score, \tilde{S}_p is median evidential class scores in proximity map p , and m is slope of the function. For the same reason of using the class median distance in Eq. 1, the median of evidential class scores is used instead of the mean of evidential class scores in Eq. 2. A suitable value of m is determined by trial-and-error until the steepest part of the graph fSc versus distance has a slope similar to the slope of the steepest part of the graph Sc versus distance. Application of Eq. 2 results in normalization of evidential class scores in every proximity map to the same range [0,1], which is meaningful because in poorly-explored areas the significance of every geological feature in terms of mineralization may not be well-known *a-priori*. Thus, the transformation of Sc into fSc also serves to reduce/remove bias due to differences in statistical distributions of data.

Maps of fSc for each set of geological features are then input to principal components (PC) analysis to obtain a mineral prospectivity function representing a linear combination of the evidential variables. Interpretation of a particular PC (or eigenvector) as a linear function representing mineral prospectivity is based on the multivariate association between different evidential variables, as indicated by the magnitude and signs of the eigenvector loadings. The geological meaning of multivariate association of evidential scores represented by each PC is

interpreted in terms of mineralization significance according to conceptual models or knowledge of geological characteristics of the deposit-type sought. A score map of the PC interpreted to represent a mineral prospectivity function is generated and considered as a predictive map of mineral prospectivity. The methodology is validated by evaluating performance of the predictive map of mineral prospectivity according to the procedures described by Agterberg and Bonham-Carter (2005)

Results

The values of S_c and fS_c derived for classes of proximity to each set of geological features are given in Appendix 1. The suitable slope used in Eq. 2 is 200. Fig. 2 is an example illustration of effect of transforming S_c into fS_c . The values of S_c suggest narrow zones of mineral prospectivity at and around geological features, whereas the values of fS_c suggest slightly broader zones of mineral prospectivity at and around geological features. The variation of S_c with distance from geological features is suitable for vein-type deposits, but the variation of fS_c with distance from geological features is more appropriate for porphyry-type deposits.

The results of PC analysis of the fuzzified evidential scores of proximity classes are given in Table 1. The PC1 is a plausible porphyry-Cu prospectivity function. It reflects association between heat controls (granodiorite batholith margins, quartz diorite porphyry stock centroids), structural controls (N- and NE-trending faults, intersections of N- and NE-trending faults), and Cu anomalies. The PC3 is also a plausible porphyry-Cu prospectivity function. It reflects associations between heat controls (granodiorite batholith margins, quartz diorite porphyry stock centroids), structural controls (NW-trending faults), and Cu anomalies. In contrast to the PC1, the PC3 shows higher positive contributions by granodiorite batholith rather than by quartz diorite porphyry stocks. However, it is known generally that porphyry-Cu deposits are genetically associated with porphyry stocks rather than igneous batholiths (Titley and Beane, 1981). Therefore, the PC1 is favoured over the PC3 as the better representation of a porphyry-Cu prospectivity function.

Table 1. Principal component analysis of fuzzified evidential scores of classes of proximity to geological features and geochemical anomalies. GB = granodiorite batholith margins. QDB = quartz diorite batholith margins. QDPS = quartz diorite porphyry stock centroids. NW = NW-trending faults. NE = NE-trending faults. N = N-trending faults. Cu = drainage catchment basins with Cu anomalies.

	GB	QDB	QDPS	NW	NE	N	FI	Cu	Var. (%)	∑ Var. (%)
PC1	0.329	0.101	0.423	-0.062	0.212	0.463	0.512	0.420	27.39	27.39
PC2	-0.166	-0.626	0.054	0.588	0.306	0.131	0.227	-0.263	18.11	45.50
PC3	0.530	-0.168	0.180	0.479	-0.321	-0.257	-0.342	0.377	14.27	59.77
PC4	-0.308	-0.053	0.013	0.120	-0.781	0.523	0.063	-0.001	12.69	72.46
PC5	-0.680	0.135	0.132	0.208	0.173	-0.163	-0.110	0.625	9.06	81.52
PC6	-0.050	0.633	0.448	0.430	-0.015	-0.106	0.055	-0.443	7.08	88.60
PC7	0.154	0.383	-0.701	0.411	0.189	0.341	-0.036	0.126	6.56	95.16
PC8	0.005	0.041	-0.275	0.093	-0.286	-0.524	0.740	0.097	4.84	100.00

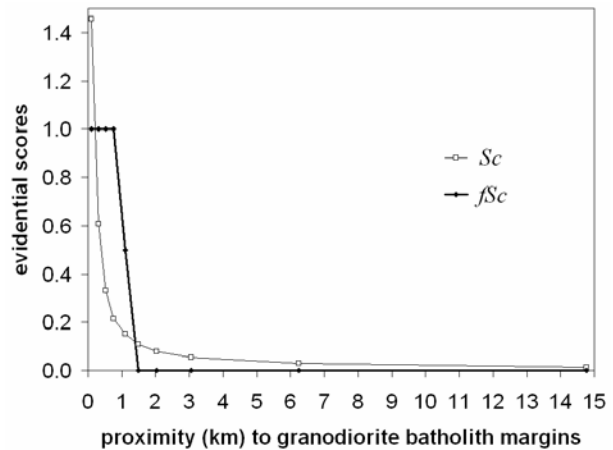


Fig. 2. Variation of evidential scores (S_c) and fuzzified evidential scores (fS_c) with proximity to granodiorite batholith margins in Abra area.

The other PCs are not plausible porphyry-Cu prospectivity functions. The PC2 represents associations between quartz diorite batholith and Cu anomalies, which are antipathetic to associations between faults. The PC4 mainly represent association between granodiorite batholith margins and NE-trending faults, which is antipathetic to N-trending faults. The PC5 reflects antipathetic relation between granodiorite batholith margins and Cu anomalies. The PC6 reflects antipathetic association of Cu anomalies with quartz diorite batholith margins, quartz diorite porphyry stock centroids, and NW-trending faults. The PC7 reflects mainly the quartz diorite porphyry stock centroids. The PC8 reflects mainly the intersections between N- and NE-trending faults.

Following the procedures described by Agterberg and Bonham-Carter (2005), thresholds of PC1 scores at certain percentiles were used to map different prospective zones, prediction rates of different prospective zones are determined, and then graphs of prospective zones versus prediction rates are created. Prediction rate represents percentage of either porphyry-Cu prospects or mineralized zones delineated by prospective zones. Analysis of the prediction rate graphs (Fig. 3) indicate that the study area can be classified into high and low geothermal prospectivity zones (Fig. 4). A slight inflection (flattening) of the prediction rates curve based on mineralized zones at about 35% prospective zones was basis for setting boundary between high and low prospectivity zones. High prospectivity zones have PC1 scores greater than 1.3112, occupy 35% of the study area, and have 67-77% prediction rates. Low prospectivity zones have PC1 scores less than 1.3112, occupy 65% of the study area, and have 23-33% prediction rates.

Discussion and conclusions

The choice of geological features to be used as spatial evidences in predictive mapping of mineral

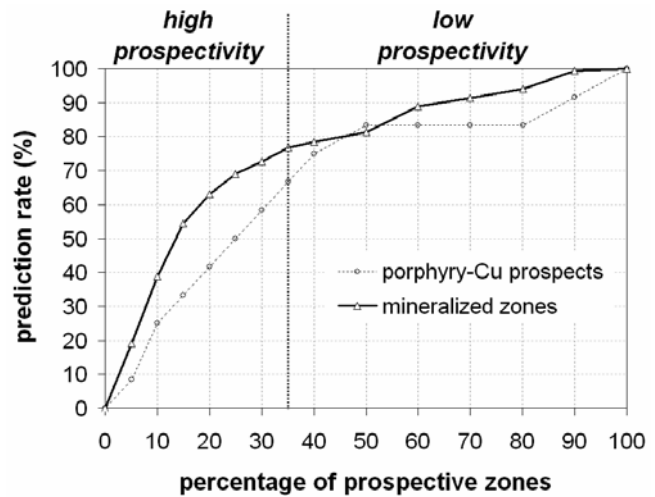


Fig. 3. Prediction rates of porphyry-Cu prospectivity map.

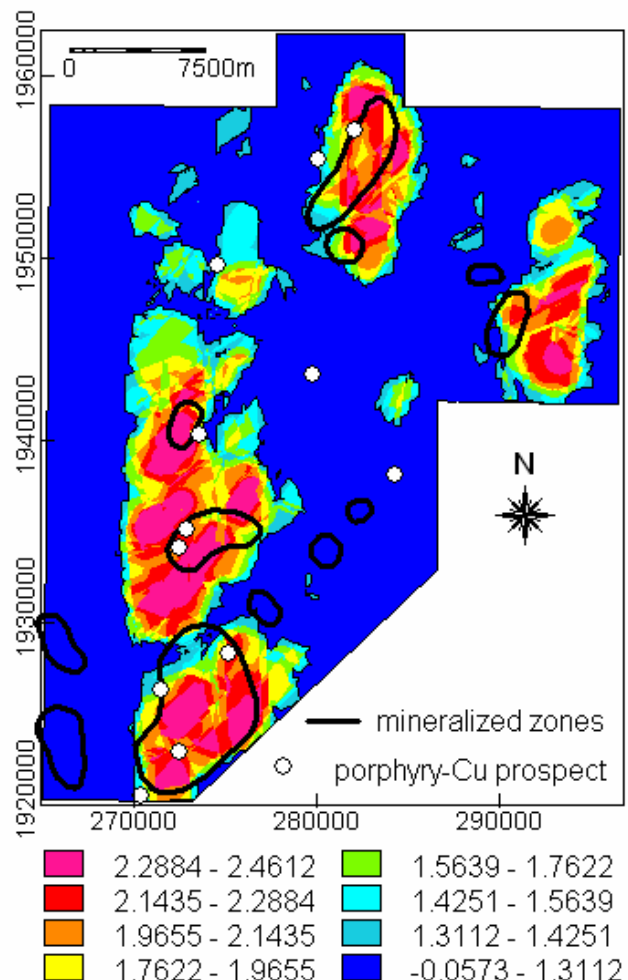


Fig. 4. Porphyry-Cu prospectivity map based on modified wildcat method. Thin lines represent boundary between high and low prospectivity zones.

prospectivity is based on (a) conceptual models of mineral deposits of the type sought (e.g., Titley and Beane, 1981) and/or (b) general characteristics of mineral deposits of the type sought in similar geological settings. In this study, the choice of geological features used in the modified wildcat mapping of porphyry-Cu prospectivity in the Abra was based on previous work by Carranza and Hale (2002b) on weights-of-evidence predictive mapping of porphyry-Cu prospectivity in Benguet (Philippines).

In areas with no known discovered mineral deposits of the type sought, performance of a predictive map of mineral prospectivity can be evaluated only through fieldwork. However, the evaluation of performance of the porphyry-Cu prospectivity map presented here based on known porphyry-Cu prospects and mineralized provides an empirical validation of the proposed modified wildcat technique. The earlier work of Carranza (2004) on weights-of-evidence predictive mapping of porphyry-Cu prospectivity resulted in delineation of prospectivity zones occupying 30% of the same study area and a corresponding 73% prediction rate. Based on results in this study, if high prospectivity zones occupying 30% of the study area are considered, then prediction rate is 58-73% (Fig. 3). This illustrates usefulness of the modified wildcat technique in predictive mapping of mineral prospectivity in geologically-permissive areas with no or few discovered mineral deposits of the type sought. Predictive mineral prospectivity map derived by using the modified wildcat technique can be used to guide further exploration in delineated prospective zones.

References

- Agterberg, F.P., Bonham-Carter, F., 2005. Measuring performance of mineral-potential maps. *Natural Resources Research* 14, 1-17.
- Carranza, E.J.M., 2004. Weights of evidence modeling of mineral potential: a case study using small number of prospects, Abra, Philippines. *Natural Resources Research* 13, 173-187.
- Carranza, E.J.M., Hale, M., 2002a. Spatial association of mineral occurrences and curvilinear geological features. *Mathematical Geology* 34, 203-221.
- Carranza, E.J.M., Hale, M., 2002b. Where are porphyry copper deposits spatially localized? A case study in Benguet province, Philippines, *Natural Resources Research* 11, 45-59.
- Carranza, E.J.M., Hale, M., 2002c. Wildcat mapping of gold potential, Baguio district, Philippines. *Transactions of Institution of Mining and Metallurgy, Section B – Applied Earth Science* 111, B100-B105.
- Porwal, A., Carranza, E.J.M. and Hale, M., 2003. Knowledge-driven and data-driven fuzzy models for predictive mineral potential mapping. *Natural Resources Research* 12, 1-25.
- Titley, S. R., Beane, R. E., 1981, Porphyry copper deposits – Part I: Geological settings, petrology and tectogenesis: *Economic Geology 75th Anniversary Volume (Special Volume)*, 214–235.

Brief bio-data of author

E.J.M. Carranza is B.Sc. in geology (Adamson University, Philippines, 1983), M.Sc. in mineral exploration [International Institute for Geo-Information Science and Earth Observation (ITC), The Netherlands, 1994], and Ph.D. in mineral exploration (Delft University of Technology, Netherlands, 2002). He was mineral exploration geologist in the Mines and Geosciences Bureau of the Philippines (1983-2001). He was a Researcher (2001-2003) and now an Assistant Professor at ITC.



Appendix 1. Evidential class scores and fuzzified evidential class scores of proximity to geological features.

Evidential map	\tilde{d}_c	S_c	\tilde{S}	fS_c
<i>Classes of proximity (m) to granodiorite batholith margins</i>				
0 – 100	96.8	1.4566	0.1517	1.0000
100 – 300	232.3	0.6070	0.1517	1.0000
300 – 530	425.9	0.3311	0.1517	1.0000
530 – 760	658.2	0.2142	0.1517	1.0000
760 – 1100	929.3	0.1517	0.1517	0.5000
1100 – 1480	1297.1	0.1087	0.1517	0.0002
1480 – 2020	1761.8	0.0800	0.1517	0.0000
2020 – 3060	2555.5	0.0552	0.1517	0.0000
3060 – 6240	4665.8	0.0302	0.1517	0.0000
6240 – 14760	10493.1	0.0134	0.1517	0.0000
<i>Classes of proximity (m) to quartz diorite batholith margins</i>				
0 – 550	367.8	0.3834	0.0450	1.0000
550 – 1240	909.9	0.1550	0.0450	1.0000
1240 – 2020	1645.6	0.0857	0.0450	0.9997
2020 – 2770	2400.6	0.0587	0.0450	0.9393
2770 – 3470	3136.3	0.0450	0.0450	0.5000
3470 – 4210	3852.6	0.0366	0.0450	0.1571
4210 – 5060	4646.4	0.0303	0.0450	0.0502
5060 – 6050	5556.3	0.0254	0.0450	0.0195
6050 – 7340	6698.6	0.0210	0.0450	0.0082
7340 – 10710	9041.1	0.0156	0.0450	0.0028
<i>Classes of proximity (m) to quartz diorite porphyry stock centroids</i>				
0 – 1200	716.3	0.1968	0.0366	1.0000
1200 – 1980	1587.5	0.0888	0.0366	1.0000
1980 – 2680	2342.6	0.0602	0.0366	0.9912
2680 – 3450	3078.2	0.0458	0.0366	0.8629
3450 – 4240	3852.6	0.0366	0.0366	0.5000
4240 – 5040	4646.4	0.0303	0.0366	0.2210
5040 – 5850	5459.5	0.0258	0.0366	0.1034
5850 – 6820	6350.1	0.0222	0.0366	0.0532
6820 – 8200	7511.7	0.0188	0.0366	0.0277
8200 – 13150	10667.4	0.0132	0.0366	0.0092
<i>Classes of proximity (m) to drainage Cu anomalies</i>				
0 – 150	96.8	1.4566	0.0958	1.0000
150 – 570	406.6	0.3468	0.0958	1.0000
570 – 940	755.0	0.1868	0.0958	1.0000
940 – 1280	1122.9	0.1256	0.0958	0.9974
1280 – 1650	1471.4	0.0958	0.0958	0.5000
1650 – 2080	1877.9	0.0751	0.0958	0.0157
2080 – 2620	2361.9	0.0597	0.0958	0.0007
2620 – 3320	2981.4	0.0473	0.0958	0.0001
3320 – 4300	3813.9	0.0370	0.0958	0.0000
4300 – 7920	6117.8	0.0230	0.0958	0.0000

Appendix 2. continuation

Evidential map	\tilde{d}_c	S_c	\tilde{S}	fS_c
<i>Classes of proximity (m) to NW-trending faults</i>				
0 – 570	387.2	0.3642	0.0532	1.0000
570 – 1130	851.8	0.1655	0.0532	1.0000
1130 – 1670	1413.3	0.0998	0.0532	0.9999
1670 – 2250	1974.7	0.0714	0.0532	0.9744
2250 – 3030	2652.3	0.0532	0.0532	0.5000
3030 – 4000	3523.5	0.0400	0.0532	0.0666
4000 – 5120	4569.0	0.0309	0.0532	0.0114
5120 – 6650	5885.4	0.0240	0.0532	0.0029
6650 – 8830	7744.0	0.0182	0.0532	0.0009
8830 – 15180	12003.2	0.0117	0.0532	0.0002
<i>Classes of proximity (m) to NE-trending faults</i>				
0 – 150	96.8	1.4566	0.1776	1.0000
150 – 350	271.0	0.5202	0.1776	1.0000
350 – 520	425.9	0.3310	0.1776	1.0000
520 – 660	600.2	0.2349	0.1776	1.0000
660 – 900	793.8	0.1776	0.1776	0.5000
900 – 1150	1026.1	0.1374	0.1776	0.0003
1150 – 1480	1316.5	0.1071	0.1776	0.0000
1480 – 1920	1703.7	0.0828	0.1776	0.0000
1920 – 2660	2303.8	0.0612	0.1776	0.0000
2660 – 7520	5072.3	0.0278	0.1776	0.0000
<i>Classes of proximity (m) to N-trending faults</i>				
0 – 200	135.5	1.0406	0.1214	1.0000
200 – 470	367.8	0.3834	0.1214	1.0000
470 – 660	580.8	0.2428	0.1214	1.0000
660 – 950	813.1	0.1734	0.1214	1.0000
950 – 1340	1161.6	0.1214	0.1214	0.5000
1340 – 1730	1548.8	0.0910	0.1214	0.0023
1730 – 2210	1974.7	0.0714	0.1214	0.0000
2210 – 2830	2536.2	0.0556	0.1214	0.0000
2830 – 3650	3252.5	0.0434	0.1214	0.0000
3650 – 6970	5285.3	0.0267	0.1214	0.0000
<i>Classes of proximity (m) to intersections of N- and NE-trending faults</i>				
0 – 760	503.4	0.2801	0.0728	1.0000
760 – 1100	929.3	0.1517	0.0728	1.0000
1100 – 1400	1258.4	0.1120	0.0728	0.9996
1400 – 1730	1568.2	0.0899	0.0728	0.9683
1730 – 2120	1936.0	0.0728	0.0728	0.5000
2120 – 2560	2342.6	0.0602	0.0728	0.0745
2560 – 3080	2826.6	0.0499	0.0728	0.0102
3080 – 3780	3446.1	0.0409	0.0728	0.0017
3780 – 4880	4336.6	0.0325	0.0728	0.0003
4880 – 8680	6776.0	0.0208	0.0728	0.0000